A Simulation of the Magnetic Resonance Elastography Steady State Wave Response through Idealised Atherosclerotic Plaques

Lauren E. J. Thomas-Seale, Dieter Klatt, Pankaj Pankaj, Neil Roberts, Ingolf Sack
and Peter R. Hoskins

Abstract— **The clinical assessment of the rupture risk of atherosclerotic plaque is made by imaging the reduction of the lumen; via ultrasound or angiography. It is known that this is an imperfect criterion and that other characteristics of the plaque, such as the change in mechanical properties, may be more relevant. Magnetic Resonance Elastography (MRE) is a novel imaging technique that measures tissue stiffness. Magnetic resonance imaging measures the tissue displacement in response to harmonic shear waves excited on the surface of the body by a vibrating actuator. The images of wave propagation are transformed into an image of stiffness using an inversion algorithm. A steady state analysis was conducted on a simulation of MRE shear waves propagating through an idealised atherosclerotic plaque. The variation of the 2D complex wave response was investigated with regards to stenosis size, lipid pool size and excitation frequency. The detectability of small lipid pools was shown to increase with frequency. However significant wave disruptions were observed at higher excitation frequencies. This study shall form the basis for future work on incorporating an inversion algorithm into the simulation.**

Index Terms—**Atherosclerosis, finite element analysis, magnetic resonance elastography, plaque rupture, shear waves.**

I. INTRODUCTION

Cardiovascular disease (CVD) encompasses a wide range of debilitating and lethal pathologies including stroke, coronary heart disease, abdominal aortic aneurysms and heart failure. Twenty nine percent of mortalities in the world and 38% in the UK are caused by CVD [1] and of these nearly three quarters have the underlying cause of atherosclerosis [2].

The symptoms of atherosclerosis depend largely upon the affected artery. As the disease develops the plaque begins to form a stenosis; a narrowing of the lumen which affects the blood flow. The more serious consequences of atherosclerosis, stroke and heart attack, are caused by the rupture of these plaques restricting blood flow to the brain and heart respectively. The clinical diagnosis of atherosclerotic plaque severity is made by imaging the reduction of the lumen; via ultrasound or angiography. The percent stenosis of a plaque, as per the European Carotid Surgery Trail (ESCT), is calculated as the ratio of the minimum diameter of the stenosed artery to an estimate of the original width [3].

A carotid endarterectomy is the standard surgical treatment for symptomatic carotid stenosis; it is considered beneficial for stenosis between 70% and 99% [4]. However it is widely accepted that using stenosis size as a criteria for surgery is imperfect diagnosis technique. The results of the ESCT show an absolute beneficial increase of surgery, for stenosis greater than 80%, of 11.6% [3]. Hence, approximately nine surgical interventions are conducted to ensure that one patient will be stroke free after 3 years [3].

A large variety of research is focussed on improving the assessment of atherosclerotic plaque rupture risk; inflammation markers detected by magnetic resonance imaging (MRI) of ultra-small superparamagnetic nanoparticles of iron oxide [5], changes in plaque geometry imaged using multispectral MRI [6], estimation of plaque stress using image guided modelling [7] and changes in mechanical properties [8]. It is the imaging of mechanical properties which forms the basis behind this research.

It has been established that there are intrinsic differences between stable and unstable plaques. Plaques which are vulnerable to rupture have a similar morphology; a thin fibrous cap over a large lipid pool core [9]. Plaque rupture depends upon the strength of the plaque withstanding the force from the blood flow [10]. With vulnerable plaque morphology, a large proportion of low stiffness lipid results in the forces from the blood flow being primarily supported by the fibrous cap; when the strength of this is exceeded the plaque ruptures [9]. Depending on the imaging technique, plaque composition can be detected to various degrees of resolution. However plaque strength cannot be accurately

L. E. J. Thomas-Seale is with Medical Physics, University of Edinburgh, Chancellor's Building, 49 Little France Crescent, Edinburgh, EH16 4SB, UK (phone: +44 131 2426307; e-mail: L.E.J.Thomas@sms.ed.ac.uk).

D. Klatt is with the MR Elastography Group, Charité Universitätsmedizin Berlin, Charitéplatz 1, 10117 Berlin, Germany. (e-mail: dieter.klatt@charite.de)

P. Pankaj is with the School of Engineering, University of Edinburgh, Alexander Graham Bell Building, The King's Buildings, Edinburgh EH9 3JL, UK (e-mail: Pankaj@ed.ac.uk).

N. Roberts is with the Clinical Research Imaging Centre, University of Edinburgh, 47 Little France Crescent, Edinburgh, EH16 4SB, UK (e-mail: Neil.Roberts@ed.ac.uk).

I. Sack is with the MR Elastography Group, Charité Universitätsmedizin Berlin, Charitéplatz 1, 10117 Berlin, Germany. (e-mail: ingolf.sack@charite.de)

P. Hoskins is with Medical Physics, University of Edinburgh, Chancellor's Building, 49 Little France Crescent, Edinburgh, EH16 4SB, UK (email: P.Hoskins@ed.ac.uk)

determined by composition alone because the properties of the lipid and fibrous cap can vary [11], [12].

Magnetic Resonance Elastography (MRE) combines MRI with elastography; a tissue elasticity imaging technique. MRI has high spatial and temporal resolution, which is ideally suited to measuring tissue displacement in response to propagating harmonic waves in the range of 10-1000Hz [13]. MRE uses phase contrast MRI to capture the steady state propagation of the waves through the tissue at a series of time offsets corresponding to a fraction of the excitation frequency [14]. The phase differences images are then combined and temporally Fourier transformed to create a complex wave image corresponding to the excitation frequency [14]. These wave images form the input to a technique known as wave inversion, yielding an image of stiffness known as an elastogram.

It is hypothesised that MRE could have the potential to non-invasively assess the stiffness of an atherosclerotic plaque and hence provide an improved indication of the rupture risk. Beyond the exploration of 1D MRE shear wave behaviour through atherosclerotic plaques [15], there has been no other research involving MRE analysis of plaque stiffness. Only limited literature exists on the application of MRE to arteries; to identify wall stiffness [16], [17], [18], [19] and stenosis size using reflected and transmitted waves [16].

Computational simulation allows cost and time efficient assessment of the limitations and optimisation of the proposed technique. An initial investigation into the transient shear wave behaviour though an atherosclerotic plaque with disease development suggested that MRE could have the potential to differentiate between plaques of varying lipid volumes [15]. This paper focuses on the complex displacement images of steady state wave propagation, compatible with MRE wave inversion techniques, as opposed the previously discussed transient results [15]. The aim of this paper is to investigate the 2D steady state behaviour of shear waves through various atherosclerotic plaque compositions at a range of frequencies.

II. METHOD

A. Overview

A MRE simulation was performed using finite element analysis (FEA) to create a complex wave image synonymous to that gained during an experimental scan. This may be demonstrated by comparing Fig. 1 (a) a flow chart of the MRE procedure, with Fig. 1 (b) a flow chart of the simulation methodology. The dashed arrows in Fig. 1 (b) represent the steps not included in this paper. A steady state frequency response analysis was conducted at the corresponding wave excitation frequency. Simulations were conducted at a range of loading frequencies and plaque compositions.

The model geometry was created using the computer aided design software RHINO Version 3.0, McNeel, Seattle, Washington, USA. Simulations were conducted using the finite element modelling software ABAQUS CAE Version 6.8-1, Simulia, Providence, Rhode Island, USA. Data formatting was conducted using the programming software MATLAB R2011a, MathWorks, Natick, Massachusetts, USA.

B. Geometry

The simulation geometry comprised of an idealised atherosclerotic plaque embedded in a three layered, straight vessel surrounded by a block of tissue. The vessel wall
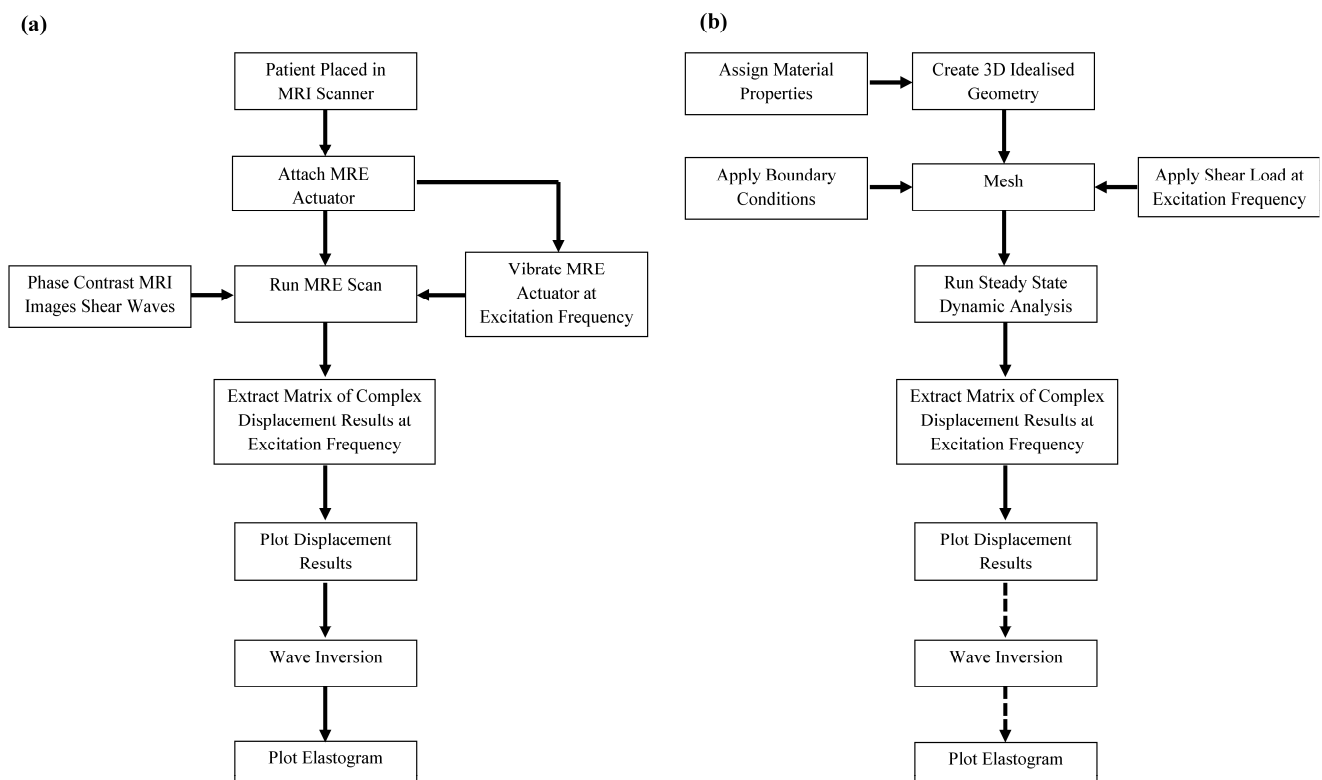
(a)

```
Patient Placed in
MRI Scanner
      │
      ▼
Attach MRE ──────────────┐
Actuator                 │
      │                  ▼
      │            Vibrate MRE
Phase Contrast MRI ──→ Run MRE Scan ←── Actuator at
Images Shear Waves                   Excitation Frequency
      │
      ▼
Extract Matrix of Complex
Displacement Results at
Excitation Frequency
      │
      ▼
Plot Displacement
Results
      │
      ▼
Wave Inversion
      │
      ▼
Plot Elastogram
```

(b)

```
Assign Material ──────→ Create 3D Idealised
Properties              Geometry
                              │
                              ▼
Apply Boundary ────────→ Mesh ←──── Apply Shear Load at
Conditions                          Excitation Frequency
                              │
                              ▼
                      Run Steady State
                      Dynamic Analysis
                              │
                              ▼
                 Extract Matrix of Complex
                 Displacement Results at
                 Excitation Frequency
                              │
                              ▼
                   Plot Displacement
                   Results
                              ┊
                              ▼
                     Wave Inversion
                              ┊
                              ▼
                     Plot Elastogram
```

Fig. 1. Flow charts of (a) the MRE procedure and (b) the simulation methodolgy

geometry is taken from [20] and detailed in Table I. The plaque was modelled as an eccentric stenosis [21], [22]. The lipid pool within the plaque was modelled as a sphere of varying volume surrounded by fibrotic intima. Fig. 2 clarifies the idealised plaque geometry, it shows cross-sectional views of an 80% stenosis containing a 25mm³ lipid pool. Surrounding tissue was incorporated into the model to replicate the transmission of shear waves in-vivo; an interface between the actuator and region of interest.

C. Material Properties

The material properties used in the simulation are detailed in Table I. The material properties of the vessel were taken from [23]; the wall was modelled as an isotropic, hyperelastic, neo-hookean material and the lipid pool as a low stiffness, incompressible solid. The surrounding tissue was modelled with linear, elastic properties [24]. The solid components of the model were modelled with an average value of density for soft tissue [24]. Damping was modelled simply over the wall and tissue using a value of 0.1 kHz, taken from previous computational simulations of MRE [25]. Blood flow through the lumen was modelled as static, with acoustic properties as described in [26]. The model was meshed using quadratic and linear tetrahedron, hybrid and acoustic elements.

D. Loads and Boundary Conditions

A sinusoidal shear load of 2 kN was applied to the nodes above the plaque on the top surface of the tissue block. Fig. 2 (c) is an isometric view of a half model, sectioned through the Y-Z plane. The global coordinates and locations of the load nodes (L) are shown; the load was applied parallel to the Z axis. Non-reflecting boundary conditions were applied to all surfaces apart from the loaded surface. These constraints were chosen to reduce the wave interference generated by waves reflected from the outer boundaries of the surrounding tissue.

E. Data Processing

The results were taken at a matrix of points, with 0.5 mm spacing, through various sectional planes of the plaque. In order to isolate the shear wave, the component of displacement in the same direction as the load, parallel to the Z axis, was taken. The results were plotted as two

TABLE I
SIMULATION PARAMETERS

Geometry	Parameter	Symbol	Value
Solid components	Density	ρ	1040kgm⁻³
	Damping	ζ	0.1kHz
Intima	Inner radius	R_I	3.63x10⁻³m
	Thickness	T_I	1.7x10⁻⁴m
	Shear modulus	μ_I	150kPa
Media	Inner radius	R_M	3.8x10⁻³m
	Thickness	T_M	7.3x10⁻⁴m
	Shear modulus	μ_M	34kPa
Adventitia	Inner radius	R_A	4.53x10⁻³m
	Thickness	T_A	4.3x10⁻⁴m
	Shear modulus	μ_A	50kPa
Fibrotic intima	Shear modulus	μ_{FI}	221kPa
Fibrous cap	Shear modulus	μ_{FC}	165kPa
Lipid pool	Young's modulus	E_L	0.3kPa
Tissue	Young's modulus	E_T	50kPa
Blood	Density	ρ_B	1060kgm⁻³
	Bulk modulus	K	2.67GPa

dimensional displacement maps; formatted as pixelated images, similar to those obtained from an experimental MRE scan. The images were created using a MATLAB program designed by the Elastography group at the Charité Hospital, Berlin.

III. RESULTS

Fig. 3 displays the real and imaginary shear wave displacement maps through a 60%, 70% and 80% stenosis containing a 20mm³ lipid pool. The models were excited and analysed at a frequency of 200Hz. Results through the Y-Z and X-Y planes are shown.

Fig. 4 shows the real component of the shear wave passing through an 80% stenosis with a range of lipid pool sizes, at a range of excitation frequencies. Results through the Y-Z plane are displayed.

Fig. 5 contains expanded images of the real component of the shear wave propagating through an 80% stenosis containing a 45mm³ lipid pool. The models were excited and analysed at 150Hz and 350Hz. The results through the Y-Z plane are shown.

IV. DISCUSSION

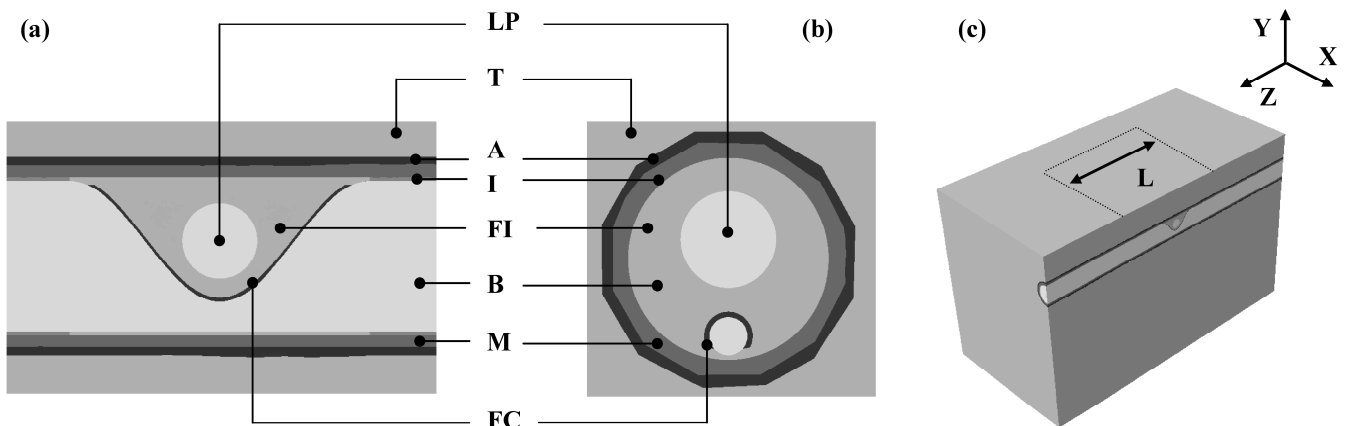Fig. 3 compares the real and imaginary displacement

Fig. 2. Sectional views of the 80% stenosis and 25mm³ lipid pool model through an (a) Y-Z and (b) X-Y plane displaying the geometry and (c) a half model through the Y-Z plane indicating the load area and direction. References are as follows: surrounding tissue T, adventitia A, media M, intima I, fibrotic intima, FI, fibrous cap FC, lipid pool LP, blood B and load L.

results from a 200Hz wave simulation through three stenosis sizes; 60%, 70% and 80%. Planar waves are very clear in both sections taken through the Y-Z and X-Y planes. The complex displacement may be described using the interchangeable terms of modulus and phase or real and imaginary components. The modulus is the magnitude of the displacement and the phase is generated by damping. It was decided to display the results in terms of the real and imaginary components so that the wave images would appear with a larger range of displacements, both positive and negative, to provide improved clarity.

In all images there is zero displacement in the lumen because fluids do not transmit shear waves [25]. The lipid pool shows peaks of displacement similar to the results obtained in [15]. In the Y-Z plane the waves show a drop in amplitude once they have propagated below the plaque and lumen. A corresponding drop in amplitude can be seen in the X-Y plane images.

Comparing the results between the stenosis sizes; the distinguishing feature between the 60%, 70% and 80% images is the absence of displacement in the lumen. As previously mentioned there are already well established methods for imaging the narrowing of the lumen caused by a stenosis. Since the aim of this research is to develop MRE as a method of assessing plaque stiffness not size, the rest of the results neglected variation in stenosis and focussed upon imaging the variation in lipid pool size. In addition the results concentrated on images of the real component of displacement in the Y-Z plane, primarily for image clarity.

Fig. [4] shows the shear wave propagation through an 80% stenosis containing various lipid pool sizes, at a range of excitation frequencies. The visualisation of the lipid pool varies with lipid pool size and frequency. MRE literature describes the limitations of excitation frequency as a trade-off between wavelength and attenuation. Whilst the lower threshold of excitation frequency is limited by the detectability capacity of the wavelength, the higher threshold is limited by attenuation [27, 28]. The low detectability of smaller lipid pools at low excitation frequencies is clearly demonstrated in Fig. 4. The 5mm^3 lipid pool is virtually invisible at 100Hz and 150Hz. At 100Hz the 15mm^3 lipid

pools remains extremely faint. Once the excitation frequency is 200Hz or above, all the lipid pool sizes become visible.

Up until 150Hz the peaks of a local wave within the lipid pool, similar to those seen in the transient analysis of [15], are visible. However at frequencies of 200Hz and above there is a loss of continuity between the wave patterns as the lipid pool varies in size. At 350Hz there are also differences in the behaviour of the wave propagating through the surrounding tissue, where the only physical difference between the models is the lipid pool size. Fig. 5 shows an expanded image of the wave displacement passing through a 45mm^3 stenosis at 150Hz and 350Hz. The wave propagation in the 350Hz simulation appears highly disrupted compared to the planar waves in the 150Hz simulation.

$$c_s = \sqrt{\frac{\mu}{\rho}} \qquad (1)$$

MRE literature suggests that wave reflections are often observed during in-vivo studies and constitute a drawback in the technique [27]. The disruption of wave propagation can be highly undesirable as in some cases the inversion algorithm incorporates the assumption of planar waves [29]. It is hypothesized that as the excitation frequency increases, the disruptions seen in Fig. [5] are caused by increased amounts of wave reflection; as the wavelength reduces it becomes more comparable to the geometric lengths in the model. For example, using the shear wave speed, c_s calculation (1) from [30]; at 200Hz the approximate wavelength through the surrounding tissue is 20mm and the lipid pool is 0.5mm. There are certain frequency values, notably 200Hz and 350Hz; that show overall larger wave amplitudes. There are also intermittent lipid pool sizes within Fig. 4 that contain noticeably larger or smaller wave amplitudes, compared to other lipid pools at the same excitation frequency. For example the wave amplitudes within the 15mm^3 lipid pool at 150Hz and 45mm^3 at 250Hz are comparatively high and in the 15mm^3 lipid pool at 200Hz and 55mm^3 lipid pool at 350Hz comparably low. It is hypothesized that at certain frequencies and lipid pool sizes,
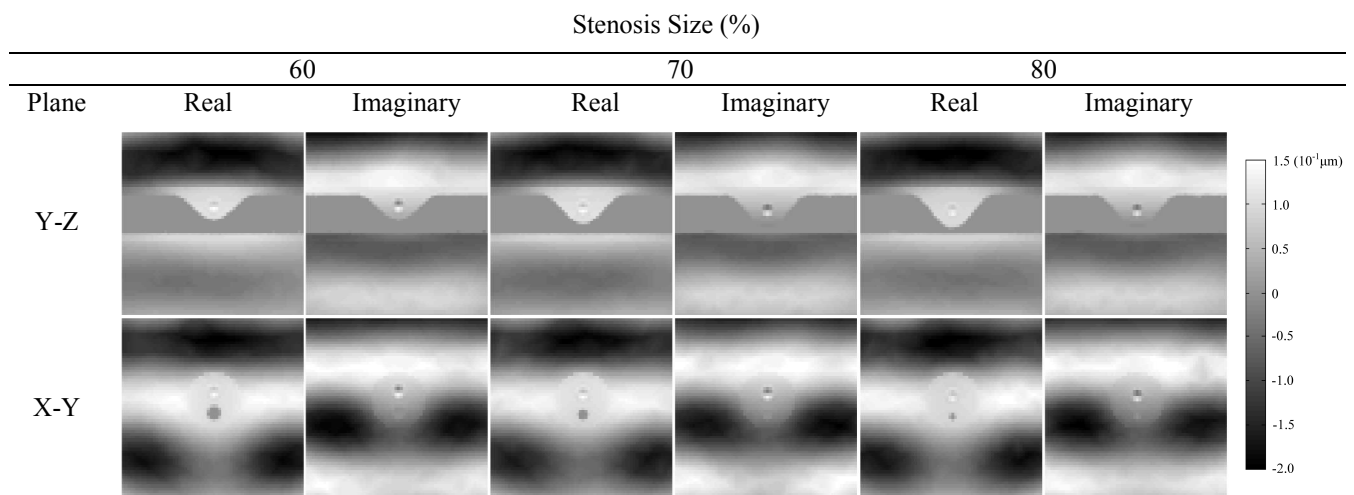
Stenosis Size (%)

Fig. 3. Complex displacement images of 200Hz shear waves propagating through a 60%, 70% and 80% stenosis containing a 20mm^3 lipid pool. Real and imaginary components of displacement are shown through the Y-Z and X-Y plane.

the interaction between the geometry and wavelength is creating either constructive or destructive wave superposition.

This study employs a very simple method of modelling damping; it is uniform across all the tissues and viscoelastic effects have also been neglected. This means that the frequency limitation imposed by attenuation cannot be assessed. To investigate the implication of attenuation in MRE simulations, these factors must be modelled more realistically. Current MRE research also involves multi-frequency studies to investigate the viscoelastic properties of tissue [31]. Incorporating realistic viscoelastic properties to the model would also allow a multi-frequency study to be conducted as well giving a more realistic indication of the excitation frequency threshold imposed by attenuation. This study has neglected the motion induced in the vessel due to the cardiac cycle. This is an applicable assumption because during an in-vivo investigation the MRI sequence would be
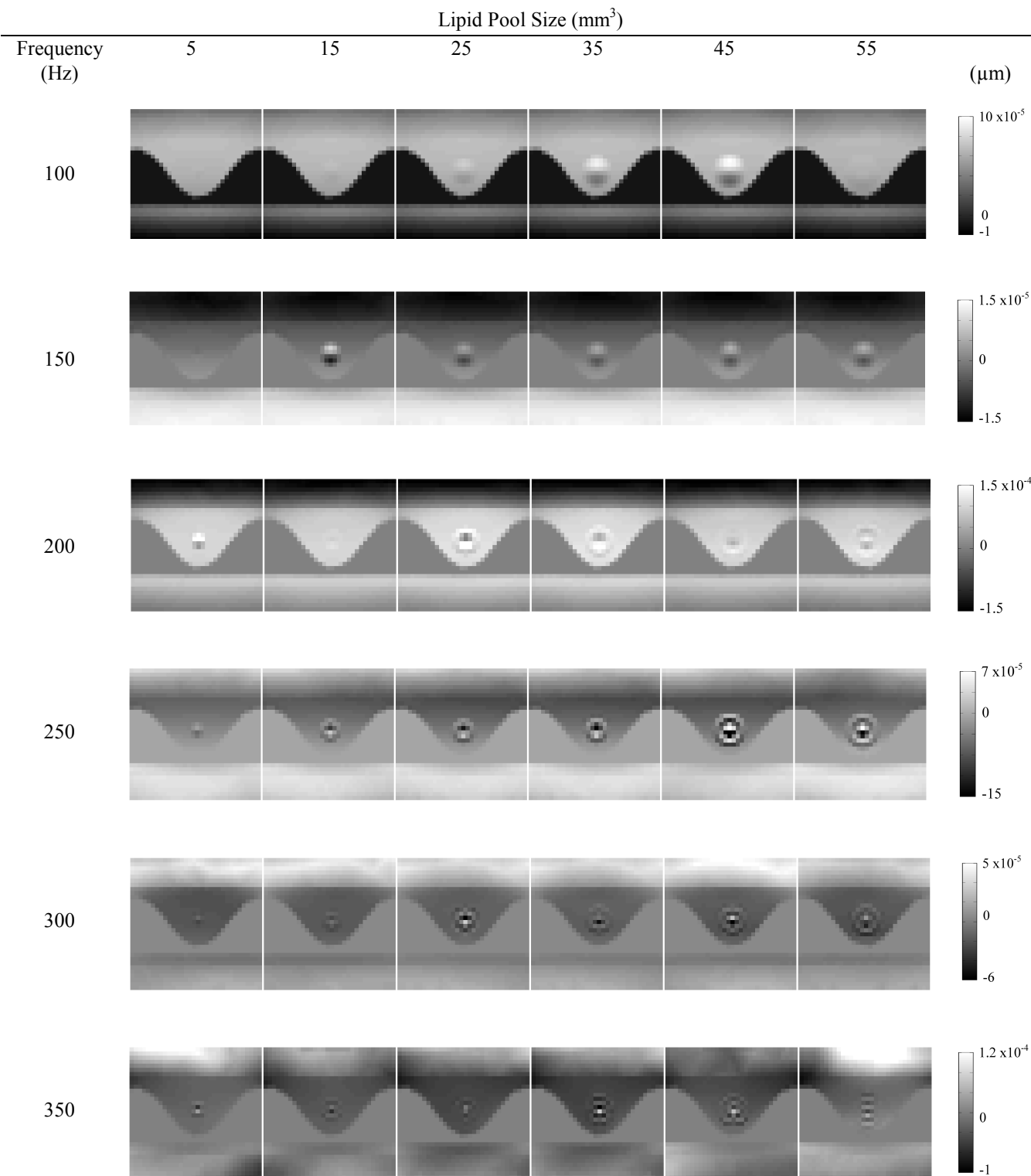

Fig. 4. Complex displacement images of shear waves propagating through an 80% stenosis containing a range of lipid pool sizes, at a range of frequencies. The real component of displacement is shown through the Y-Z plane.
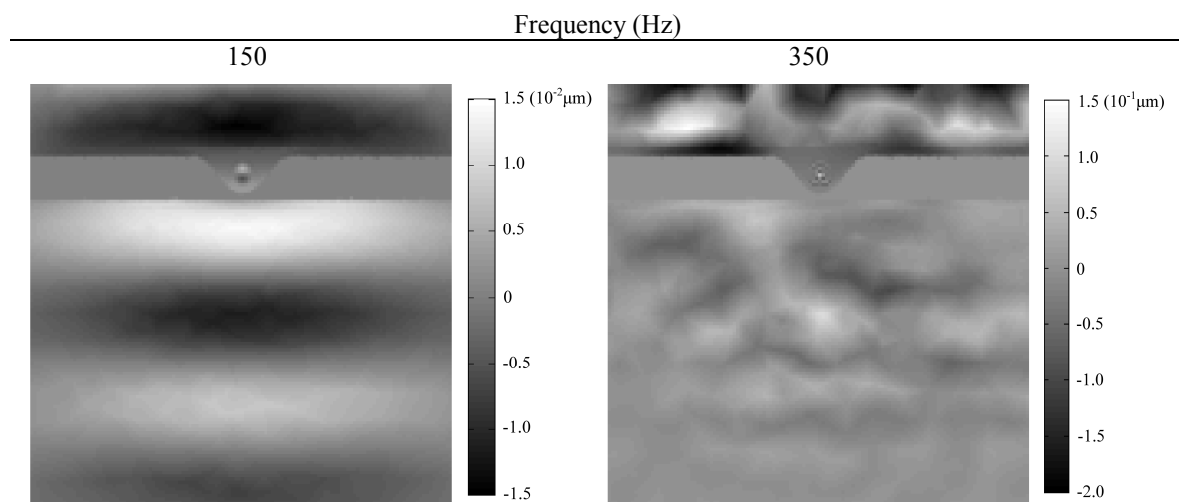
Frequency (Hz)

150   350

Fig. 5. Complex displacement images of shear waves propagating through an 80% stenosis containing a 45mm^3 lipid pool sizes, at a frequency of 150Hz and 350Hz. The real component of displacement is shown through the Y-Z plane.

gated to ensure that images are taken at the same vessel dilation. However it should be noted that during an in-vivo MRE scan of the artery the quality of the wave image would probably be reduced by flow artefacts.

V. CONCLUSION

This study has demonstrated that a proportion of the MRE technique may be simulated using FEA. It has been shown that excitation frequency and lipid pool size affect the behaviour of steady state shear complex waves passing through an idealised atherosclerotic plaque. This would suggest that the future simulation and application of MRE to atherosclerosis may be able to identify plaque stiffness and improve clinical diagnosis of rupture risk.

REFERENCES

[1] C. D. Mathers, C. Bernard, K. M. Iburg, M. Inoue, D. Ma Fat, K. Shibuya, et al, "Global burden of disease in 2002: data sources, methods and results," *World Health Organization*, Dec. 2003.

[2] W. Rosamond, K. Flegal, G. Friday, K. Furie, A. Go, K. Greenlund, et al, "Heart disease and stroke statistics – 2007 update: A report from the American heart association statistics committee and stroke statistics subcommittee," *Circulation*, vol. 115, e96-e171, Dec. 2006.

[3] B. Farrell, A. Fraser, P. Sandercock, J. Slattery and C. P. Warlow, "Randomised trial of endarterectomy for recently symptomatic carotid stenosis: final results of the MRC European carotid surgery trail (ECST)," *Lancet*, vol. 351, pp. 1379-1387, May 1998.

[4] P. M. Rothwell, S. A. Gutnikov and C. P. Warlow, "Reanalysis of the final results of the European carotid surgery trail," *Stroke*, vol. 34, pp. 514-523, Jan. 2003.

[5] T. Tang, S. P. S. Howarth, S. R. Miller, R. Trivedi, M. J. Graves, J. U. King-Im, et al, "Assessment of inflammatory burden contralateral to the symptomatic carotid stenosis using high-resolution ultrasmall, superparamagnetic iron oxide-enhanced MRI" *Stroke*, vol. 37, pp. 2266-2270, Sep. 2006.

[6] C. Yuan, L. M. Mitsumori, M. S. Ferguson, N. L. Polissar, D. Echelard, G. Ortiz, et al, "In vivo accuracy of multispectral magentic resonance imaging for identifying lipid-rich necrotic cores and intraplaque hemorrhage in advanced human carotid plaques" *Circulation*, vol. 104, pp. 2051-2056, Oct. 2001.

[7] Z. Y. Li, S. Howarth, R. A. Trivedi, J. M. U. King-Im, M. J. Graves, A. Brown, et al, "Stress analysis of carotid plaque rupture based on in vivo high resolution MRI" *Journal of Biomechanics*, vol. 39, pp. 2611-2622, Aug. 2006.

[8] J. J. Dahl, D. M. Dumont, J. D. Allen, E. M. Miller and G. E. Trahey, "Acoustic radiation force impulse imaging for noninvasive characterization of carotid artery atherosclerotic plaques: A feasibility study," *Ultrasound Med. Biol.,* vol. 35, pp. 707-716, May 2006.

[9] R. T. Lee and P. Libby, "The unstable atheroma," *Arterioscler. Throm. Vasc. Biol.*, vol. 17, pp. 1859-1867, Oct. 1997.

[10] E. Falk, P. K. Shah and V. Fuster, "Coronary plaque disruption," *Circulation*, vol. 92, pp. 657-671, Aug. 1995.

[11] H. M. Loree, B. J. Tobias, L. J. Gibson, R. D. Kamm, D. M. Small and R. T. Lee, "Mechanical properties of model atherosclerotic lesion lipid pools," *Arterioscler. Throm. Vasc. Biol.*, vol. 14, pp. 230-234, Feb. 1994.

[12] C. L. Lendon, M. J. Davies, G. V. R. Born and P. D. Richardson, "Atherosclerotic plaque caps are locally weakened when macrophages density is increased," *Atherosclerosis*, vol. 87, pp. 87-90, Mar. 1991.

[13] R. Muthupillai, D. J. Lomas, P. J Rossman, J. F. Greenleaf, A. Manduca and R. L. Ehamn, "Magnetic resonance elastography by direct visualization of propagating acoustic strain waves," *Science*, vol. 269, pp. 1854-1857, Sep. 1995.

[14] D. Klatt, P. Asbach, J. Rump, S. Papazoglou, R. Somasundaram, J. Modrow, et al, "In vivo determination of hepatic stiffness using steady-state free precession magnetic resonance elastography," *Investigative Radiology*, vol. 41, pp.841-848, Dec. 2006.

[15] L. Thomas-Seale, P. Pankaj, N. Roberts and P. Hoskins, "Computational modelling of magnetic resonance elastography shear wave behaviour through atherosclerotic plaque with disease development," Lecture Notes in Engineering and Computer Science: Proceedings of The World Congress of Engineering 2011, WCE 2011, 6-8 July, London, U.K., pp. 2636-2639.

[16] D. A. Woodrum, A.J. Romano, A. Lerman, U. H. Pandya, D. Brosh, P.J. Rossman, et al, "Vascular wall elasticity measurement by magnetic resonance imaging," *Magn. Reson. Med.*, vol. 56 pp. 593-600, Aug. 2006.

[17] D. A. Woodrum, J. Herrmann, A. Lerman, A. J. Romano, L. O. Lerman and R. L. Ehman, "Phase contrast MRI-based elastography technique detects early hypertensive changes in ex vivo porcine aortic wall," *J. Magn. Reson. Imaging*, vol. 29, pp. 583-587, 2009.

[18] Y. Zheng, Q. C. C. Chan and E. S. Yang, "Magnetic resonance elastography with twin drivers for high homogeneity and sensitivity," *in Proc. 28th IEEE EMBS Annual Int. Conf.*, New York, 2007, pp. 1916-1919.

[19] A. Kolipaka, D. A. Woodrum, K. R. Gorny, O. I. Garcia Medina, A. J. Romano and R. L. Ehman, "MR elastography of the in vivo abdominal aorta: feasibility study," in *Proc. Int. Soc. Mag. Reson. Med.* 18, Stockholm, 2010, pp. 1257.

[20] C. A. J. Schulze-Bauer, C. Mörth and G. A. Holzapfel, "Passive biaxial mechanical response of aged human iliac arteries," *J. Biomech. Eng.*, vol. 125, pp. 395-406, Jun. 2003.

[21] D. Tang, C. Yang, S. Kobayashi and D. N. Ku, "Effect of a lipid pool on the stress/strain distributions in stenotic arteries: 3-D fluid-structure interactions (FSI) models," *J. Biomech. Eng.*, vol. 126, pp. 363-370, Jun. 2004.

[22] M. Li, "Numerical simulation of blood flow and vessel wall stresses in stenosed arteries," Ph.D dissertation, Dept. Medical Physics, Edinburgh Univ., Edinburgh, UK, 2006.

[23] G. A. Holzapfel, M. Stadler and C. A. J. Schulze-Bauer, "A layer-specific three-dimensional model for the simulation of balloon

angioplasty using magnetic resonance imaging and mechanical testing," *Ann. Biomed. Eng*., vol. 30, pp. 753-767, Jun. 2002.

[24] P. R. Hoskins, K. Martin and A. Thrush, Diagnostic ultrasound: physics and equipment, 2nd ed. Cambridge Univ. Press, 2010.

[25] J. Braun, G. Buntkowsky, J. Bernarding, T. Tolxdorff and I. Sack, "Simulation and analysis of magnetic resonance elastography wave images using coupled harmonic oscillators and Gaussian local frequency estimation," *Magn. Reson. Imaging,* vol. 19, pp. 703-713, Feb. 2001.

[26] P. R. Hoskins, "Physical properties of tissues relevant to arterial ultrasound imaging and blood velocity measurement," *Ultrasound Med. Biol.*, vol. 33, pp. 1527-1539, Oct. 2007.

[27] R. Sinkus, J. Lorenzen, D. Schrade, M. Lorenzen, M. Dargatz and D. Holz, "High-resolution tensor MR elastography for breast tumour detection," *Phys. Med. Biol*., vol. 34, pp. 1649-1664, Nov. 2000.

[28] K. J. Parker, L. S. Taylor, S. Gracewski and D. J. Rubens, "A unified view of imaging the elastic properties of tissue," *J. Acoust. Soc. Am*., vol. 117, pp. 2705-2712 , May 2005.

[29] S. Papazoglou, U. Hamhaber, J. Braun and I. Sack, "Algebraic Helmholtz inversion in planar magnetic resonance elastography," *Phys. Med. Biol.,* vol. 53, pp. 3147-3158, May, 2008.

[30] E. L. Carstensen, K. J Parker and R. M. Lerner, "Elastography in the management of liver disease," *Ultrasound Med. Biol.,* vol. 34, pp. 1535-1546, Oct. 2008.

[31] D. Klatt, U. Hamhaber, P. Asbach, J. Braun and I, Sack, "Noninvasive assessment of the rheological behaviour of human organs using multifrequency MR elastography: A study of brain and liver viscoelasticity," *Phys. Med. Biol.,* vol. 52, pp. 7281-7294, Nov. 2007.